Identification and dynamics of coherent structures in a Coanda swirling jet flow

Zhu Yang[a], Victor Castaneda[b], Guven Ogus[a], Thomas Holemans[a], Maarten Vanierschot[a,c,*], Agustin Valera-Medina[b]

[a]*KU Leuven, Department of Mechanical Engineering, Group T Leuven campus, Celestijnenlaan 300, Heverlee, B-3000, Belgium*
[b]*School of Engineering, Cardiff University, 5 The Parade, Cardiff, CF24 3AA, UK*
[c]*North-West University, Material Science, Innovation and Modelling (MaSIM), Private Bag X2046, Mmabatho, 2745, South Africa*

Abstract

Swirl stabilised flows are the most common technology for gas turbine combustion stabilisation. Although success on the characterization of these flows is tangible, there are several structures that appear in such flows that are still a concern for fundamental and applied research. One of these structures is the Precessing Vortex Core (PVC), whose ambiguous characteristics make it an adequate mechanism for chemical mixing whilst being a detrimental component for thermoacoustic stabilisation. The PVC has been extensively characterised in swirling jet flows exhibiting vortex breakdown (in this study named Open Jet Flow or OJF). However this has not been the case for swirling Coanda (i.e. wall attached) Jet Flows (CoJF). Therefore, this research presents experimental work detailing the identification and visualisation of coherent structures in both types of jet flows. A generic swirl burner was fitted with a base plate in a position so that any of these two flows, OJF and CoJF, could be obtained within the same burner geometry. High speed stereo particle image velocimetry (S-PIV) was used to obtain a time-resolved flow field of each flow state at different flow rates. Two PVCs were clearly identified in both flows, one in the inner shear layer between the vortex breakdown bubble and the jet and one between the jet and the ambient. Precessing frequencies for the CoJF where ~8.5% higher (St ~0.9-1.0) than those of the OJF (St ~0.8-0.9). Spectral proper orthogonal decomposition was used to identify the coherent structures in the flow. Swirl strength (λ_{ci}^2) analysis was conducted on the coherent modes to establish quantitative and qualitative results and to produce a 3D reconstruction of the flow field. The results indicate that precessing coherent flow structures are present in wall attached Coanda swirling flows and these are similar to the structures found in swirling jet flows undergoing vortex breakdown.

Keywords:
Swirling flow; Coanda effect; Coherent structures; Particle image velocimetry

*maarten.vanierschot@kuleuven.be

1. Introduction

Swirling flows have been used for decades in the stabilisation of fast reacting flows especially in burners and gas turbine combustors [1, 2]. The important characteristics of these flows are the development of coherent structures that can anchor the flame, recirculate hot species and establish jet flows that reduce direct contact between the reaction zone and structural components. Emissions have also been mitigated with this technology thus ensuring its worldwide deployment for industrial purposes [3]. However, swirling flows also present structures that can have varied impacts on the flow field. The Precessing Vortex Core (PVC) is one of such structures present in Open Jet Flows (OJF) (i.e. unconfined jet flows) that has received vast attention in order to understand its behaviour and effects towards the flame in the last few decades [4, 5, 6]. Lucca-Negro and O'Doherty suggested that the structure improves mixing as a consequence of the creation of large turbulent scales [7]. On the contrary, Candel et al. denounce the PVC as one of the critical components in thermoacoustic instabilities, promoting heterogeneous patterns in the mixing and acoustic profiles which are detrimental to flame stabilisation [8]. Moreover, coupling of the structure with natural frequencies of the system can also lead to unwanted resonance, thus increasing undesirable emissions [9].

Syred and Beér were the first researchers identifying the PVC structure [10]. The structure appears after the occurrence of vortex breakdown [5, 11, 12] thus being highly correlated to the establishment of the Central Recirculation Zone (CRZ) [13, 14]. Although the co-existence of both structures is clear, the mechanism of interaction between them is still barely understood. Studies have been carried out to determine the fundamental equations of PVC-CRZ systems [15] and their interaction with further structures [16] suggesting that it is the stretching of the vortex, a consequence of the turbulent field, what maintains the cycle and quasi-stability of the core. Recent research has demonstrated the effects of temperature on the structure, with reduction of velocity at higher temperatures. Also, correlation between motion and stability has been demonstrated, showing the effects of co-rotation between the core and the precession of the vortex [6]. Other researchers [17, 18, 19] have also theorized and numerically or/and experimentally presented fundamental parameters under steady and transitional conditions of the structure. More recently, several groups have identified the PVC as being formed as a consequence of a global hydrodynamic instability of the mean flow triggered by an inherent flow resonance [11, 20].

Another type of exhaust flow with swirl is the Coanda Jet Flow (CoJF) which, contrary to the OJF, occurs when flow exiting the nozzle attaches to a flat surface perpendicular to the flow in the vicinity of the nozzle exit. This happens as a result of the entrainment of the surrounding stagnant air by the jet exiting the nozzle which develops a low pressure region between the surface and the jet [21]. Some fundamental research has been conducted on swirling Coanda flows. Vanoverberghe studied the transition between flow regimes by varying swirl numbers observing that swirl numbers were largely responsible for the type of flow pattern obtained [22]. Vanierschot and Van den Bulck also showed that the flow pattern was greatly dependent on the imposed swirl number, and additionally demonstrated that some hysteresis between OJF and CoJF can occur when dynamically increasing/decreasing the swirl [23, 24]. Furthermore, they showed that the nozzle geometry is an important factor in the formation of the flow pattern [25]. Singh and Ramamurthi showed that the increase in swirl in sharp-edged nozzles produces a system were centrifugal forces dominate and spread the flow in the radial direction and additionally, they identified a recirculation bubble near the nozzle exit [26]. However, despite the recent research, the complex 3D flow of the Coanda effect remains barely understood as only few researches have been conducted on the underlying coherent flow structures that might exist on the flow.

Therefore, this research is based on continuation of previous work [27] to decipher the underlying coherent structures that are present in a CoJF. The fundamental idea of the research is based on first having a particular geometry at which the system would present both flow patterns under the same inlet flow conditions, hence to be able to identify and compare the coherent structures present in each of the flow patterns. For that aim, time-resolved stereo particle image velocimetry (S-PIV) was used to produce time dependent data and subsequently spectral proper orthogonal decomposition was used to identify the coherent modes in the flow. Swirl strength (λ_{ci}^2) analysis was conducted on the coherent modes to establish quantitative and qualitative results and to produce a 3D visualisation of the coherent structures in an OJF and CoJF. This paper is structured as follows, section 2 and 3 describe the experimental setup and data processing methods. Subsequently, in section 4, the time-averaged flow patterns for different flow rates are discussed, followed by a temporal analysis of the flow fields. Finally, the principal modes of the flow are obtained by spectral proper orthogonal decomposition and the coherent structures present in the flow are identified and analysed.

2. Experimental setup

A swirl burner constructed from stainless steel was used to examine the flow field behaviour under atmospheric conditions (1 bar, 293 K). A schematic of the generic burner is presented in Fig. 1 and a more detailed description can be found in the work of Syred et al. [28]. The system was fed using compressed air through flexible hoses and variable area rotameters for flow rate control. Isothermal conditions were evaluated for these trials and the flow rate was fixed at 4.2, 6.5, 9.4 and 13.5 m^3/hr to give a Reynolds number of ~4300, ~6700, ~9600 and ~13900 respectively at the burner nozzle. The nozzle diameter was D = 28 mm with an opening angle α = 45 degrees. The burner was fitted with a tangential swirl generator providing a geometrical swirl number Sg = 0.85. A flat plate was fitted to the nozzle and kept at a normalised height $|\Delta X/D|$ = 0, being ΔX the distance between the flat plate and the tip of the nozzle outlet, for which a schematic of this can be seen in Fig. 1.
A stereo PIV system was employed for measurement purposes. A diagram of the experimental setup is shown in Fig. 2. The latter consists of a dual cavity Nd:YLF high speed laser of 532 nm wavelength. Laser sheet optics were used to convert the laser beam into a 1 mm thick sheet. To

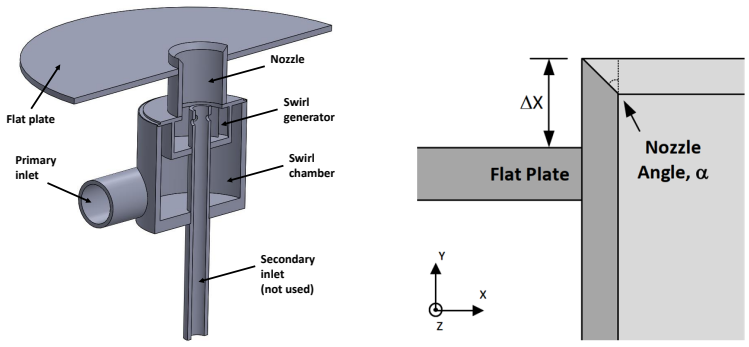

Figure 1: Swirl burner (left) and normalised height schematic (right).

record the images a pair of HighSpeedStar 5 CMOS cameras were used. 60 mm Nikon lenses were utilized for resolution purposes, which allowed a field of view of approximately 75x75 mm, with a resolution of 5.35 pixels per mm and a depth of view of 1.5 mm. The inlet air was seeded using a liquid nebulizer positioned ~2m upstream of the burner inlet. As seeding, DEHS droplets of $1\mu m$ average diameter are used which could follow to flow up to frequencies of 8kHz [29]. For the experiments, the sampling rate was set at 500, 750 and 1000 Hz. In order to reduce the parallax error, focusing was achieved using a 3D calibration plate and correcting the position of the lens (Scheimpflug correction). The line of view of the camera was positioned exactly in the middle of the nozzle. The images were recorded in double frame mode and for every Reynolds number, the time between 2 frames of the same pair was chosen to ensure a maximum particle displacement just below 1/4th of the interrogation window area and to minimise the quantity of particles leaving the measurement plane between two pulses.

3. Data processing

After acquisition of the PIV data, a frame-to-frame adaptive correlation technique was carried out with a starting interrogation area of 64x64 pixels going to a final size of 24x24 pixels. Time-averaged flow fields were calculated using 1024 velocity field samples. This gives a sampling error of about 2% on the mean flow quantities and below 6% for the second order statistics. The vector fields were also used to determine vortical structures and swirl strength values (λ_{ci}^2) during both stable flow patterns (i.e. CoJF or OJF). Data was post-processed using Matlab R2018b with the PIVMat toolbox [30]. The snapshot method was used to obtain the spectral proper orthogonal decomposition (SPOD) for each flow case to identify coherent structures within each flow pattern [31].

To isolate the fluctuations in the flow and differentiate between precessing fluctuations and fluctuations due to turbulence, a triple velocity decomposition was performed:

$$\mathbf{v}\left(x, y, t_k\right) = \overline{\mathbf{v}}\left(x, y\right) + \tilde{\mathbf{v}}\left(x, y, t_k\right) + \mathbf{v}'\left(x, y, t_k\right), \tag{1}$$

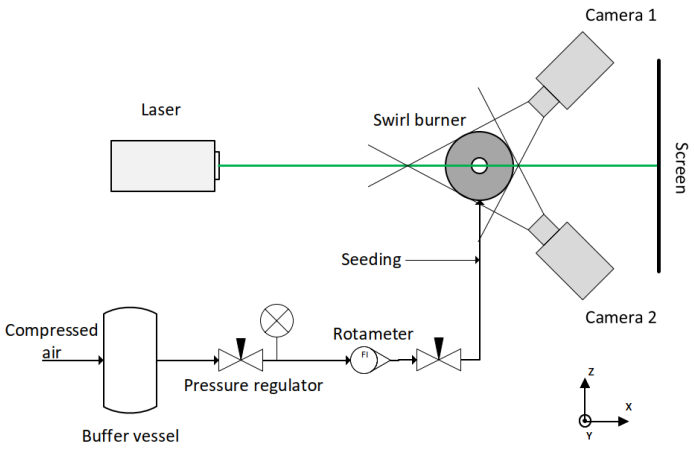

Figure 2: Schematic view of the experimental setup.

where vector $\mathbf{v}(x, y, t_k)$ is the instantaneous velocity vector at point x, y and time instant t_k, $\overline{\mathbf{v}}(x, y)$ is the mean value, $\tilde{\mathbf{v}}(x, y, t_k)$ is the fluctuation due to a precessing motion, and $\mathbf{v}'(x, y, t_k)$ is the fluctuation due to turbulence. $\tilde{\mathbf{v}}(x, y, t_k)$ was calculated by reconstructing the SPOD modes that correspond to the precessing motion and $\mathbf{v}'(x, y, t_k)$ was calculated by taking the difference of the total fluctuating velocity and the precessing velocity.

To obtain a better visualization of the coherent structures within the flow, a 3D reconstruction was done by first phase averaging the SPOD modes that correspond to the precessing motion. Then, to place the values in a 3D space, the 2D fields are rotated using an angle of rotation $\theta = 2\pi f_p/f_s$, where f_p is the precessing frequency and f_s is the sampling frequency of the 2D fields. More details about the procedure can be found in the works of Vanierschot and Ogus [32] and Oberleithner et al. [11].

4. Results and discussion

4.1. Time-averaged flow patterns

Time-averaged results were obtained for various flow rates with the flat plate at a normalised height such that both Coanda and Open Jet flows coexisted. Which pattern is stable at that height depends on the hysteresis in flow patterns between an up- and downward movement of the flat plate. When moving the plate up, an Open Jet flow is formed, while moving the plate down, a Coanda Jet flow can be obtained. For the current burner setup this corresponds to $|\Delta X/D| = 0$ with a nozzle opening angle of 45°. Vector fields of the in-plane time-averaged velocity components u_x and u_y and contours of the out-of-plane velocity component u_z are shown in Fig. 3. The u_z velocity component was scaled by the mean axial jet velocity for each case to allow a comparison of the different Reynolds numbers. The vector fields show the expected velocity profiles: a vertical jet core with a central recirculation zone for the OJF (top row of Fig. 3) and a horizontal jet core with a downward velocity at the centre of the nozzle for the CoJF (bottom row of Fig. 3). Fig. 4 shows the radial profiles of the axial velocity near the

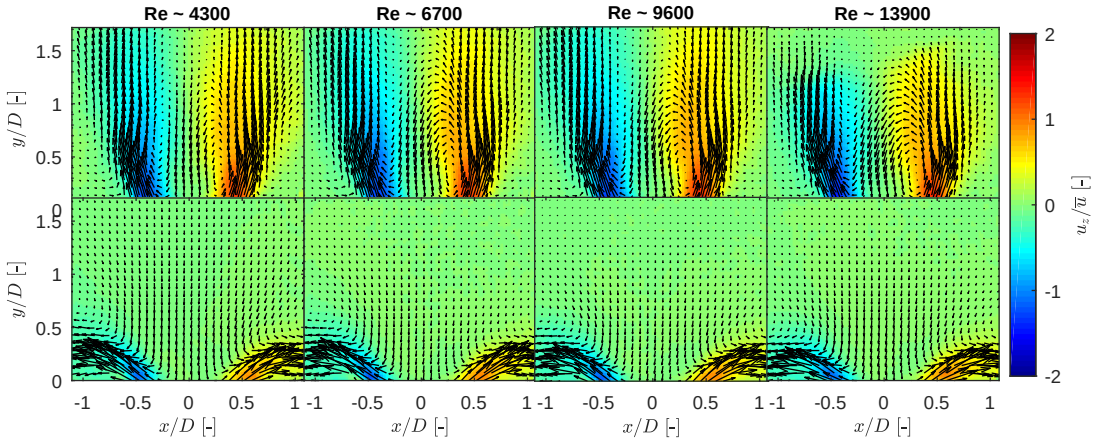

Figure 3: Time-averaged velocity fields at different flow rates with contours of the scaled out-of-plane velocity component with $|\Delta X/D| = 0$ and α=45°. Velocities are scaled by the bulk jet velocity $\overline{u}$ of each case. The top row corresponds to the OJF, while the bottom row corresponds to the CoJF.

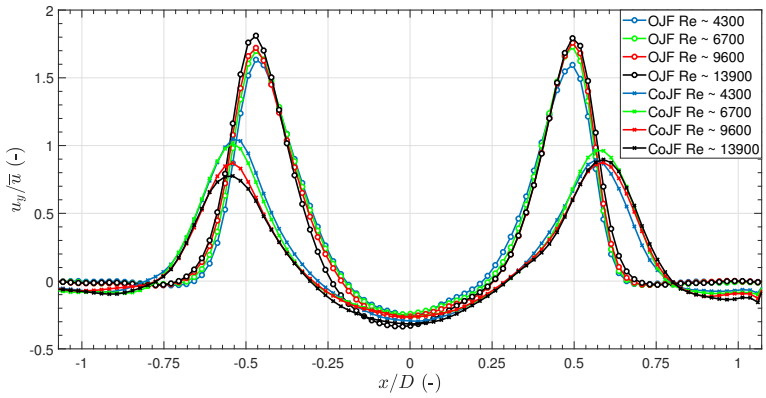

Figure 4: Scaled mean axial velocity with $|\Delta X/D| = 0$ and α=45° nozzle for different flow rates. Velocities are scaled by the bulk jet velocity $\overline{u}$ of each case.

nozzle outlet. As the Reynolds number increases, the maximum axial velocity also increases, indicating that the jet angle at the outlet decreases. For the CoJF, the opposite occurs: increasing Reynolds number decreases the maximum axial velocity. Hence, a slight decrease in jet angle at the nozzle outlet can be observed. As shown later, this increased inclination is related to a stronger attachment of the jet core to the flat plate by the appearance of a vortical structure in the outer shear layer of the jet.

4.2. Temporal power spectrum analysis

Power spectra were extracted from regions in the flow field with high RMS values. The sampling rate for the Re ~4300 and ~6700 flow rates was 500 Hz and for the Re ~9600 and ~13900 flow rates it was 750 Hz. To discard any possible aliasing, experiments were repeated with a sam-

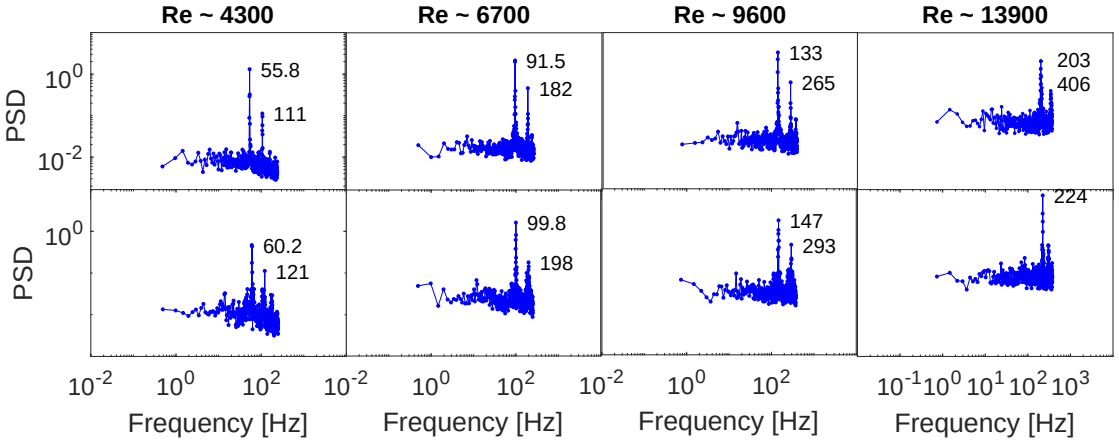

Figure 5: Power spectra of the OJF (top row) and CoJF (bottom row). 500Hz sampling rate for Re~4300 & 6700 and 750Hz for Re~9600 & 13900.

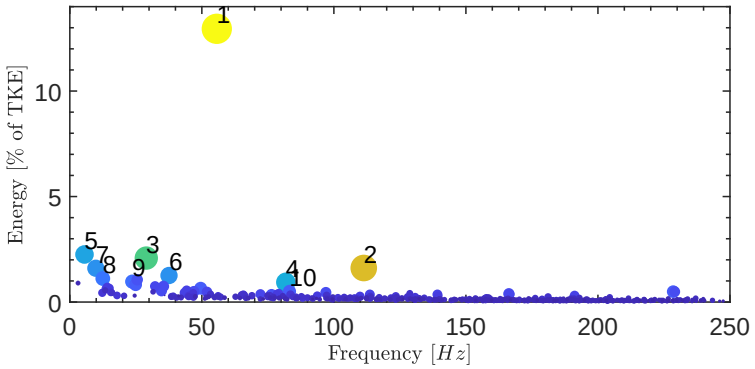

Figure 6: Spectrum of the temporal coefficients of the SPOD modes for the OJF at Re~4300.

pling rate of 1000 Hz, yielding the same results as the experiments with lower sampling rates. The power spectrum for each flow rate is shown in Fig. 5. The higher the Reynolds number, the higher the fluctuation level. Every spectrum shows two distinctive peaks. As shown in the next sections, the first frequency peak is associated to the Precessing Vortex Core and the second one corresponds to its second harmonic. The precessing frequency increases linearly with increasing Reynolds number for both the OJF and the CoJF. The range of Strouhal numbers ($\sim$ 0.8 to 1) is consistent with other studies found in literature [4]. The CoJF shows an increase in Strouhal number of ~8.5% with respect to the OJF, across all tested flow rates. It is speculated that the higher frequency in the CoJF is a consequence of its stagnation to the bottom surface, or alternatively, because another coherent structure with a higher frequency has appeared in the field, the outer PVC. This behaviour has also been previously reported in the work of Valera-Medina et al. [27].

4.3. Spectral proper orthogonal decomposition

To study the large scale coherent structures in the flow field, spectral proper orthogonal decomposition was applied to both flow patterns [31]. Previous research has shown that SPOD is better compared to POD in assigning coherent structures to different modes when applied to swirling flows [14, 32]. A filter size of one period was chosen for optimal detection of the structures [14]. An example spectrum of the time coefficients for the OJF at Re = 4300 is shown in Fig. 6. All other Reynolds numbers .show the same structure, even for the CoJF flow patterns and are hence not shown here. Two mode pairs with a high harmonic correlation can be found, one with an energy of $\sim$ 13% of the total kinetic energy and one of $\sim$ 1.6%. The high harmonic correlation indicates that both mode pairs describe precessing structures [14, 32]. The frequencies of precession of both mode pairs correspond to the peaks found in Fig. 5. Analysis of the Lissajous figures of the temporal coefficients (not shown here) indicates that the second mode pair is a first harmonic of the first mode pair. Moreover, the frequency of precession is exactly double.

The spatial structure of the first two mode pairs for the OJF are shown in Fig. 7. Several rotating structures can be found in the inner shear layer (shear layer between the jet and the central recirculation zone (CRZ), as shown in the first row of Fig. 3). These structures correspond to intersections of the Precessing Vortex Core (PVC) with the measurement plane [32] and as the

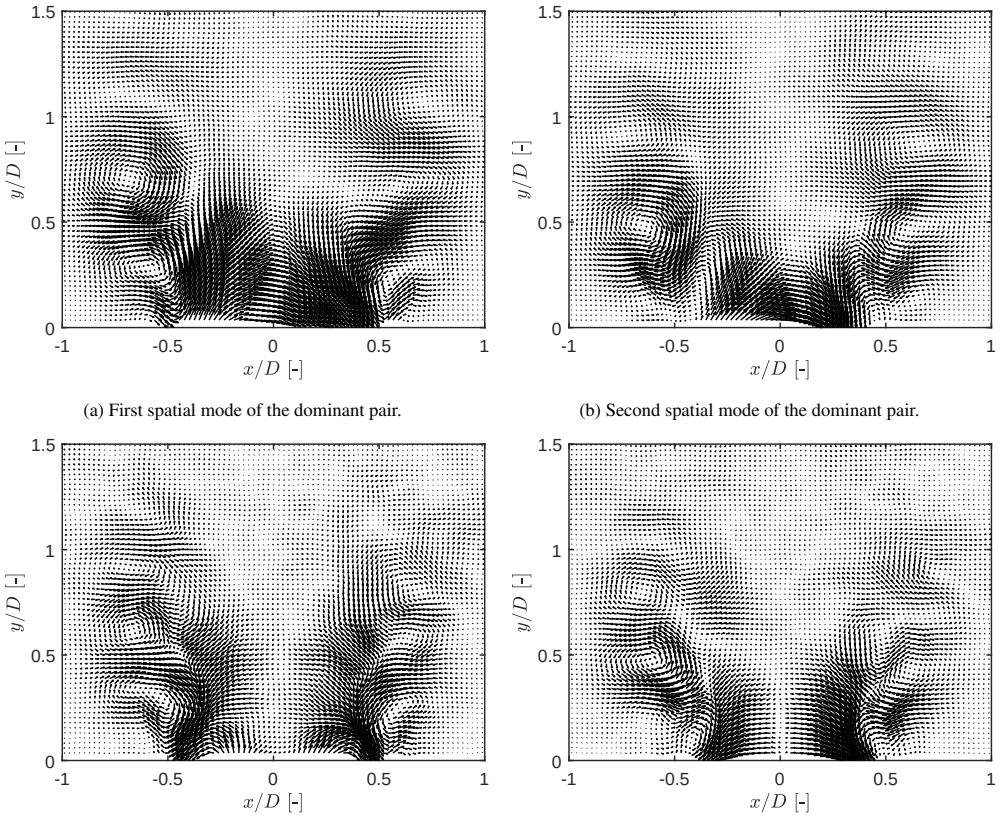

(a) First spatial mode of the dominant pair.

(b) Second spatial mode of the dominant pair.

(c) First spatial mode of the secondary pair.

(d) Second spatial mode of the secondary pair.

Figure 7: Spatial SPOD modes of the OJF.

intersections are located in the inner shear layer, this structure is often called the inner PVC [4]. The spatial modes of the CoJF (shown in Fig. 8) are very similar: several rotating structures are present due to the intersection of the PVC with the measurement plane. However, in this case, the PVC is mainly located in the outer shear layer (shear layer between jet and ambient) and hence this structure is often called the outer PVC. In the inner shear layer, the inner PVC can also be found, although being much weaker compared to the outer one.

4.4. Flow field reconstruction and flow dynamics

To study the dynamics of the flow, the 2 dominant SPOD mode pairs describing the PVC are used to obtain the velocity field $\tilde{\mathbf{v}}(x, y, t)$ in Eq. 1 and $\tilde{\mathbf{v}}(x, y, t)$ is added to the time-averaged flow field in the reconstruction, hence omitting the flow structures contained in $\mathbf{v}'(x, y, t)$. Figure 9 shows the reconstructed flow fields during the precession, where T is the period, for the OJF at Re ~4300. The vortical structures are identified using the swirl strength criterion. The same general flow behaviour and coherent structures were observed for the higher Reynolds numbers and hence the figure is representative for the dynamics in all flow cases. For the OJF case (Fig. 9) two different vortical structures can be observed, the first one in the inner shear layer of the jet and

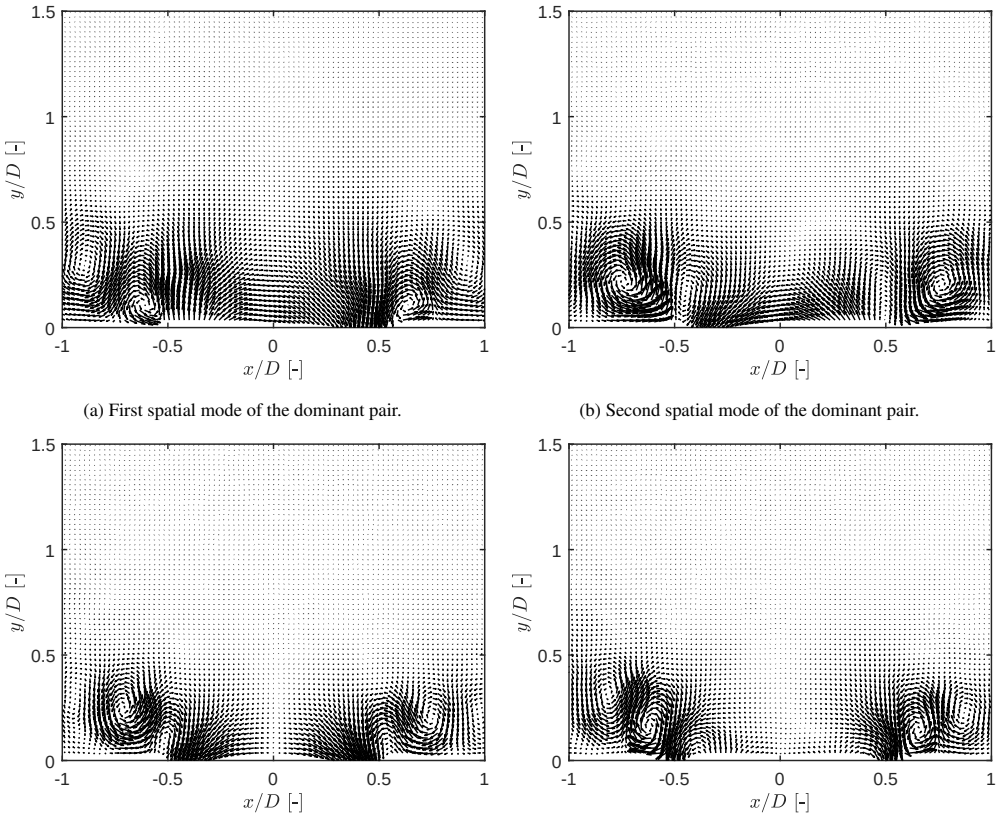

(a) First spatial mode of the dominant pair.

(b) Second spatial mode of the dominant pair.

(c) First spatial mode of the secondary pair.

(d) Second spatial mode of the secondary pair.

Figure 8: Spatial SPOD modes of the CoJF.

central recirculation zone and a second one in the outer shear layer of the jet and the ambient. These vortices correspond to intersections of the inner and outer PVC with the measurement plane and are consistent with the spatial structures found in Fig. 7. The inner PVC is stronger compared to the outer one. It originates near the nozzle at $T = 1/8$ on the negative side of the x-axis. At the next instant in the precession ($T = 1/4$), the vortex moves downstream indicating a precession of the spiral structure. As the azimuthal velocity on the left side is negative, this indicates that the windings of the PVC are oriented in the counter-swirl direction, as found by many other studies [7, 14, 32]. As the PVC spiral continues to rotate, the inner vortex loses strength and moves along the y-axis until it practically disappears at $T = 5/8$ and a new vortical structure appears near the nozzle on the positive side of the x-axis. This right intersection has the same dynamics as the initial left one and the cycle repeats itself. At $T = 1/2$, an outer vortex starts appearing into the measured plane on the negative side of the x-axis. This vortex is less strong compared to the inner one and corresponds to the outer PVC. As it continues to rotate, this vortex moves along the y-axis and loses strength as it almost disappears after one period of precession. Half a period later, at T, the intersection of the outer PVC can be found near the nozzle on the positive x-axis. This vortex also move downstream, reducing its strength.

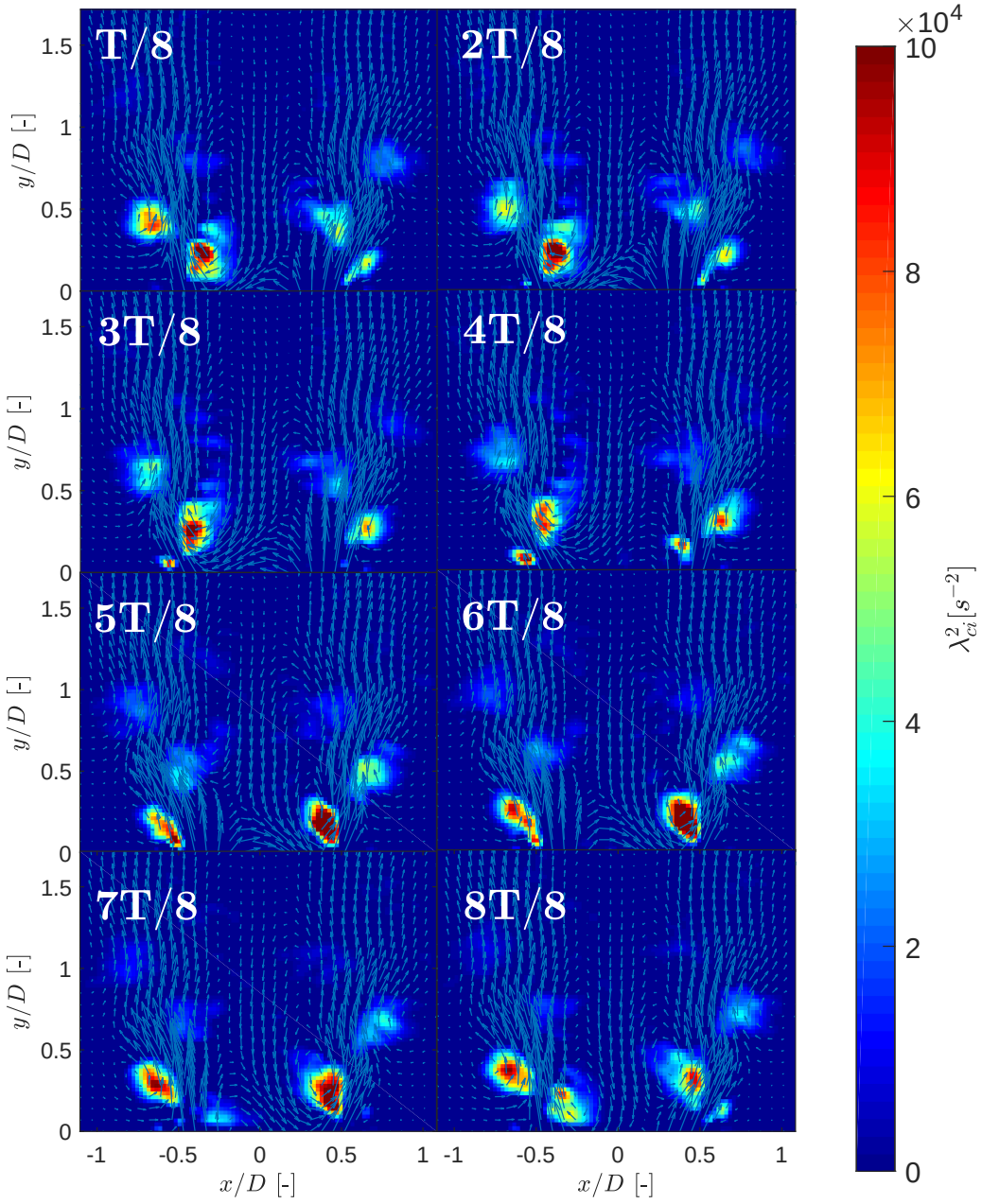

Figure 9: Time series of SPOD reconstruction of Open Jet Flow with velocity vectors and swirl strength (λ_{ci}^2) contours.

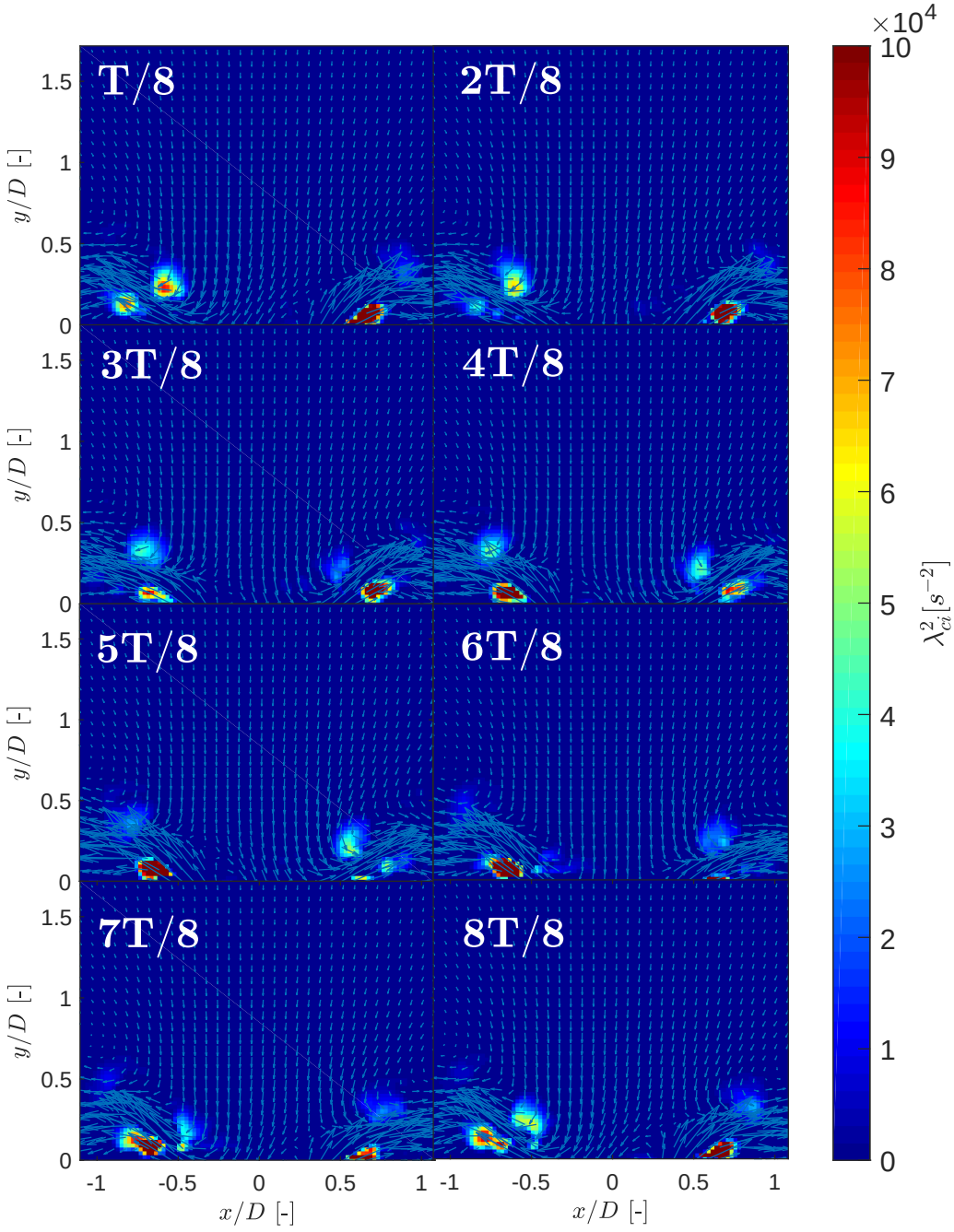

Figure 10: Time series of SPOD reconstruction of Coanda Jet Flow with velocity vectors and swirl strength (λ_{ci}^2) contours.

The Coanda Jet Flow case (Fig. 10) also shows two different vortical structures. However, in contrast to the OJF, the strongest vortex is located between the plate and the jet core in the outer shear layer. This vortical structure keeps the jet attached to the bottom wall by means of the Coanda effect. It has previously been identified as a Coanda Vortex Breakdown (CoVB), which is a product consequence of the pressure, recirculation and swirling motion of the flow [27]. The centre of the vortex has a pressure minimum, keeping the jet attached to the wall [23, 33]. As time passes, the vortex precesses around the central axis and if it cuts the measurement plane, a detachment of the jet from the plate can be observed ($T = 1/8$). Half a period later ($T = 5/8$), the vortex intersection with the measurement plane shows a very weak vortex and the jet remains attached to the plate. This strong interaction of the PVC with the wall is responsible for the slightly higher precessing frequencies, as shown in Fig. 5. Next to the outer PVC, a weaker second vortex is appearing in the inner shear layer, which is similar to the inner PVC of the OJF, thus creating a CoVB pair [27].
From the viewpoint of the PVC, the laser plane is rotating along the central axis. From these rotating intersections, the 3D structure of the PVC can be reconstructed, as detailed in the work of Vanierschot and Ogus [32]. This 3D reconstruction is shown in Fig. 11. In the figures, the central recirculation zone (CRZ) is delimited by an isosurface of axial velocity = 0 m/s (black colour). The isosurface of $u_y/\overline{u} = 0.6$ (yellow contour) is also shown to clearly mark the region between inner and outer PVC. Both inner and outer PVCs are depicted by a red isosurface with a swirl strength of $\lambda_{ci}^2 = 5000\,1/s^2$. The inner PVC is located between the CRZ and the isosurface $u_y/\overline{u} = 0.6$ and the outer one in the shear layer of the jet with the ambient. Similar structures have been found in other swirling flow geometries [34, 35]. As the swirl direction is counter-clockwise when viewed from the y-axis, both PVCs are winded in the counter-swirl direction (as could also be observed in Fig. 9). As the size of the isosurface $\lambda_{ci}^2 = 5000\,1/s^2$ of the inner PVC is smaller, one can see that the strength is higher than the outer PVC. A 3D reconstruction of the CoJF is shown in Fig. 12. In the same way as in the OJF case, the isosurface of $u_y/\overline{u} = 0.6$ (yellow colour) marks the region between inner and outer PVC. Similar to the OJF, two vortical structures can be observed by delimiting the isosurface with a swirl strength = 5,000 $1/s^2$. Both PVCs are winded in the counterswirl direction and in contrast to the OJF, the outer PVC is the strongest vortex.

4.5. Triple velocity decomposition

Triple velocity decomposition root-mean-square (RMS) values of both flow patterns are shown in Figs. 13 and 14. Very high values (up to 150% of the mean jet velocity $\overline{u}$) can be found in the inner and outer shear layers of the jet. Precessing RMS fluctuations indicate the region of coherent vortex shedding with ∼65% and ∼55% of the fluctuations attributed to the precessing phenomena for both OJF and CoJF, respectively. If the Reynolds number increases, this relative contribution remains more or less constant. However, the turbulent contribution increases with increasing Reynolds number, as can also be seen in the spectra of Fig. 5.

5. Conclusions

This paper studied the flow dynamics of two flow patterns, an Open Jet Flow (OJF) and Coanda Jet Flow (CoJF), using 2D3C-PIV in a generic swirl burner. The burner was equipped with a base plate, which can be positioned so that both flow patterns could coexist within the same geometry. Which pattern is stable at that position depends on the hysteresis in flow patterns between an up- and downward movement of the base plate. When moving the plate up, an

OJF is formed, while moving the plate down, a CoJF can be obtained. The measurements were conducted at different Reynolds numbers ranging from ~4300 to ~13900 at the burner nozzle. A spectral analysis was conducted to identify the dominant frequencies of the flow and two frequency peaks were found for each flow case. The frequency of these peaks increases linearly with the Reynolds number. Coherent flow structures were identified by spectral proper orthogonal decomposition and the frequency of the most energetic modes matched the spectral results. Reconstruction of the flow field showed that the frequency peaks corresponded to the Precessing Vortex Core (PVC), where two PVCs were found: one in the inner and one in the outer shear layer. For the OJF case, the former is the strongest one, while for the CoJF case, the latter was much stronger. This strong vortex is dominant and changes the precession frequency of the PVC being lower in the OJF case than in the CoJF by about 8.5%. The impact of the PVC on the dynamics of the flow field is significant as in some regions up to 65% of the fluctuating velocity component can be attributed to the precessing structure. Moreover, this contribution is found to be independent on the Reynolds number of the flow.

Acknowledgments

VC gratefully acknowledges a PhD scholarship from CONACYT, stipend support from TATA Steel, and the support from Cardiff University through its SeedCorn program for short secondment at KU Leuven. Also, the funding of this research by the 'Dienst onderzoekscoördinatie (DOC) KU Leuven' through grant number C3/19/015 is gratefully acknowledged.

References

[1] S. Burmberger, T. Sattelmayer, Optimization of the Aerodynamic Flame Stabilization for Fuel Flexible Gas Turbine Premix Burners, Journal of Engineering for Gas Turbines and Power 133 (10) (2011) 101501. doi:10.1115/1.4003164.
URL http://gasturbinespower.asmedigitalcollection.asme.org/article.aspx?articleid=1429528

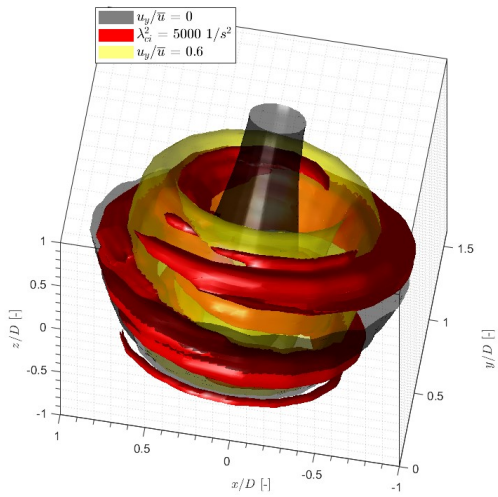

Figure 11: 3D reconstruction of the OJF.

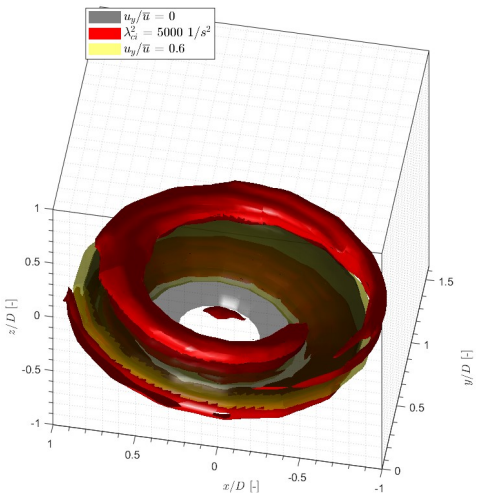

Figure 12: 3D reconstruction of the CoJF.

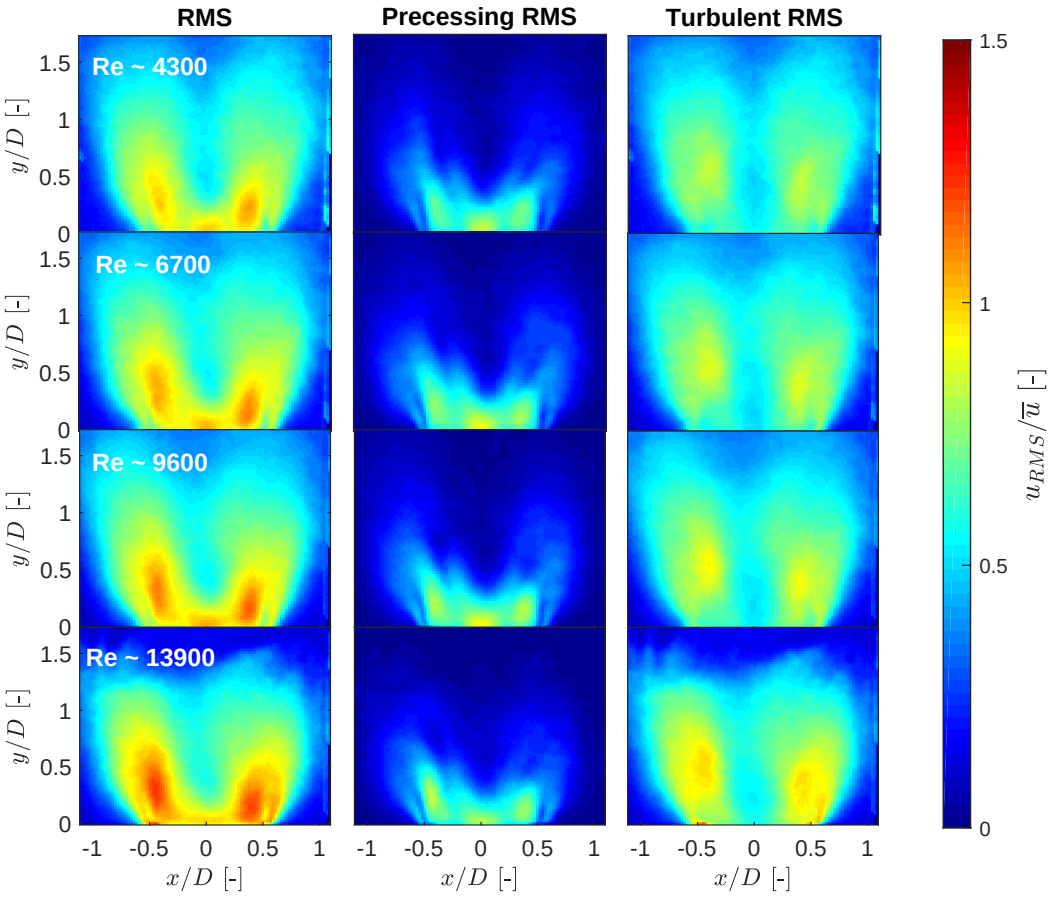

Figure 13: Scaled triple velocity decomposition time-averaged RMS fields of the OJF at Re ~4300 with $|\Delta X/D|$ = 0.000 and α=45° nozzle.

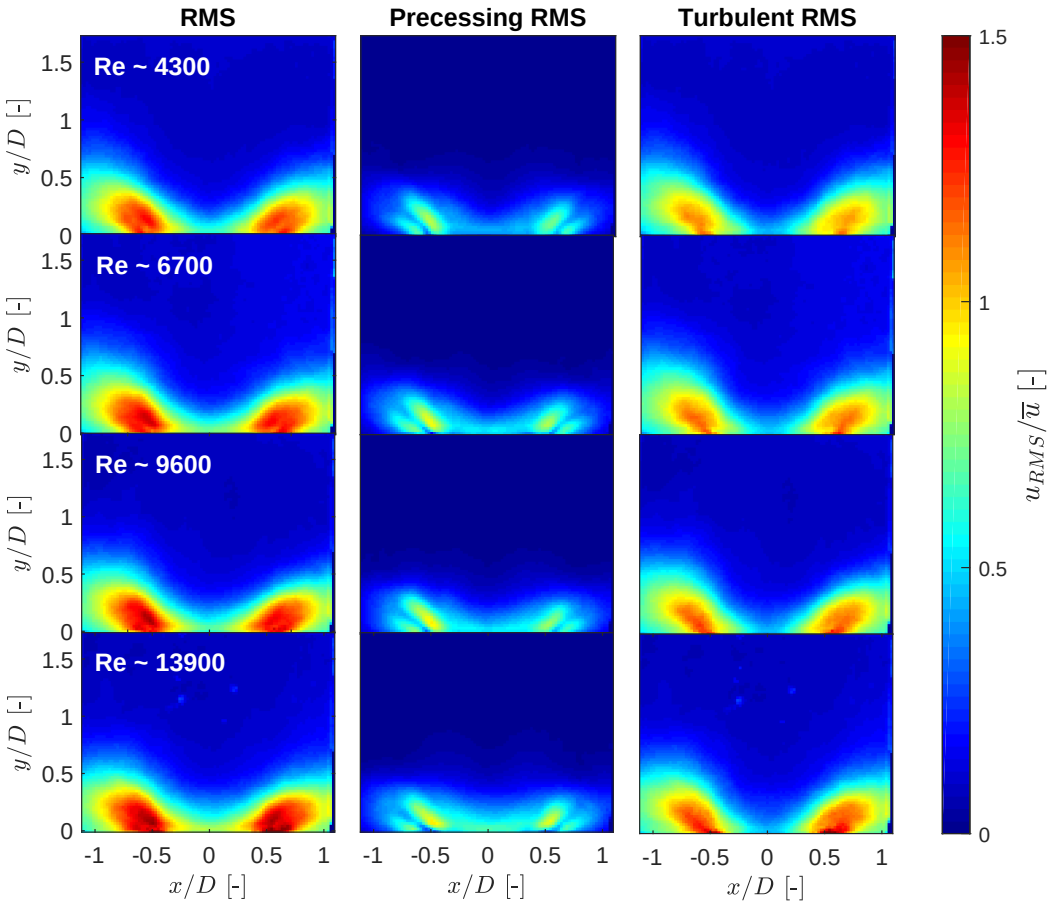

Figure 14: Scaled triple velocity decomposition time-averaged RMS fields of the CoJF t Re ~4300 with $|\Delta X/D|$ = 0.000 and α=45° nozzle.

[2] I. Chterev, G. Sundararajan, J. M. Seitzman, T. C. Lieuwen, Precession Effects on the Relationship Between Time-Averaged and Instantaneous Swirl Flow and Flame Characteristics, in: Volume 4A: Combustion, Fuels and Emissions, ASME, 2015, p. V04AT04A061. doi:10.1115/GT2015-42768.
URL http://proceedings.asmedigitalcollection.asme.org/proceeding.aspx?doi=10.1115/GT2015-42768

[3] A. Renaud, S. Ducruix, P. Scouflaire, L. Zimmer, Experimental Study of the Interactions Between Air Flow Rate Modulations and PVC in a Swirl-Stabilised Liquid Fuel Burner, in: Volume 4A: Combustion, Fuels and Emissions, ASME, 2015, p. V04AT04A063. doi:10.1115/GT2015-42775.
URL http://proceedings.asmedigitalcollection.asme.org/proceeding.aspx?doi=10.1115/GT2015-42775

[4] N. Syred, A review of oscillation mechanisms and the role of the precessing vortex core (PVC) in swirl combustion systems, Progress in Energy and Combustion Science 32 (2) (2006) 93–161. doi:10.1016/J.PECS.2005.10.002.
URL https://www.sciencedirect.com/science/article/pii/S0360128505000353

[5] A. Valera-Medina, N. Syred, A. Griffiths, Visualisation of isothermal large coherent structures in a swirl burner, Combustion and Flame 156 (9) (2009) 1723–1734. doi:10.1016/J.COMBUSTFLAME.2009.06.014.
URL https://www.sciencedirect.com/science/article/abs/pii/S0010218009001643

[6] A. Gorbunova, A. Klimov, N. Molevich, I. Moralev, D. Porfiriev, S. Sugak, I. Zavershinskii, Precessing vortex core in a swirling wake with heat release, International Journal of Heat and Fluid Flow 59 (2016) 100–108. doi:10.1016/J.IJHEATFLUIDFLOW.2016.03.002.
URL https://www.sciencedirect.com/science/article/pii/S0142727X16300182

[7] O. Lucca-Negro, T. O'Doherty, Vortex breakdown: a review, Progress in Energy and Combustion Science 27 (4) (2001) 431–481. doi:10.1016/S0360-1285(00)00022-8.
URL https://www.sciencedirect.com/science/article/pii/S0360128500000228

[8] S. Candel, D. Durox, T. Schuller, J. F. Bourgouin, J. P. Moeck, Dynamics of Swirling Flames, Annual Review of Fluid Mechanics 46 (1) (2014) 147–173. doi:10.1146/annurev-fluid-010313-141300.
URL http://www.annualreviews.org/doi/10.1146/annurev-fluid-010313-141300

[9] S. Candel, Combustion dynamics and control: Progress and challenges, Proceedings of the Combustion Institute 29 (1) (2002) 1–28. doi:10.1016/S1540-7489(02)80007-4.
URL https://www.sciencedirect.com/science/article/pii/S1540748902800074

[10] N. Syred, J. Beér, Combustion in swirling flows: A review, Combustion and Flame 23 (2) (1974) 143–201. doi:10.1016/0010-2180(74)90057-1.
URL https://www.sciencedirect.com/science/article/abs/pii/0010218074900571

[11] K. Oberleithner, M. Sieber, C. N. Nayeri, C. O. Paschereit, C. Petz, H.-C. Hege, B. R. Noack, I. Wygnanski, Three-dimensional coherent structures in a swirling jet undergoing vortex breakdown: stability analysis and empirical mode construction, Journal of Fluid Mechanics 679 (2011) 383–414. doi:10.1017/jfm.2011.141.
URL http://www.journals.cambridge.org/abstract_S0022112011001418

[12] U. A. Qadri, D. Mistry, M. P. Juniper, Structural sensitivity of spiral vortex breakdown, Journal of Fluid Mechanics 720 (2013) 558–581. doi:10.1017/jfm.2013.34.
URL http://www.journals.cambridge.org/abstract_S0022112013000347

[13] J. O'Connor, T. Lieuwen, Recirculation zone dynamics of a transversely excited swirl flow and flame, Physics of Fluids 24 (7) (2012) 075107. doi:10.1063/1.4731300.
URL http://aip.scitation.org/doi/10.1063/1.4731300

[14] M. Vanierschot, J. S. Müller, M. Sieber, M. Percin, B. W. van Oudheusden, K. Oberleithner, Single- and double-helix vortex breakdown as two dominant global modes in turbulent swirling jet flow, Journal of Fluid Mechanics 883 (2020).

[15] S. V. Alekseenko, P. A. Kuibin, V. L. Okulov, S. I. Shtork, Helical vortices in swirl flow, Journal of Fluid Mechanics 382 (1999) S0022112098003772. doi:10.1017/S0022112098003772.
URL http://www.journals.cambridge.org/abstract_S0022112098003772

[16] S. V. Alekseenko, P. A. Kuibin, S. I. Shtork, S. G. Skripkin, M. A. Tsoy, Vortex reconnection in a swirling flow, JETP Letters 103 (7) (2016) 455–459. doi:10.1134/S002136401607002X.
URL http://link.springer.com/10.1134/S002136401607002X

[17] M. Stöhr, K. Oberleithner, M. Sieber, Z. Yin, W. Meier, Experimental Study of Transient Mechanisms of Bistable Flame Shape Transitions in a Swirl Combustor, Journal of Engineering for Gas Turbines and Power 140 (1) (2017) 011503. doi:10.1115/1.4037724.
URL http://gasturbinespower.asmedigitalcollection.asme.org/article.aspx?doi=10.1115/1.4037724

[18] T. C. Lieuwen, Unsteady Combustor Physics, Cambridge University Press, Cambridge, 2012. doi:10.1017/CBO9781139059961.
URL http://ebooks.cambridge.org/ref/id/CBO9781139059961

[19] A. A. Gavrilov, A. A. Dekterev, A. V. Sentyabov, Modeling of swirling flows with coherent structures using the unsteady Reynolds stress transport model, Fluid Dynamics 50 (4) (2015) 471–482. doi:10.1134/S001546281504002X.

URL http://link.springer.com/10.1134/S001546281504002X
[20] F. Gallaire, M. Ruith, E. Meiburg, J. M. Chomaz, P. Huerre, Spiral vortex breakdown as a global mode, Journal of Fluid Mechanics 549 (-1) (2006) 71. doi:10.1017/S0022112005007834.
URL http://www.journals.cambridge.org/abstract_S0022112005007834
[21] C. Lubert, On Some Recent Applications of the Coanda Effect to Acoustics, in: Proceedings of Meetings on Acoustics, Vol. 11, Acoustical Society of America, 2012, p. 040006. doi:10.1121/1.3694201.
URL http://asa.scitation.org/doi/abs/10.1121/1.3694201
[22] K. Vanoverberghe, Flow, turbulence and combustion of premixed swirling jet flames, Ph.D. thesis, KU Leuven (2004).
URL https://limo.libis.be/primo-explore/fulldisplay?docid=LIRIAS1745178&context=L&vid=Lirias&search_scope=Lirias
[23] M. Vanierschot, E. Van den Bulck, Hysteresis in flow patterns in annular swirling jets, Experimental Thermal and Fluid Science 31 (6) (2007a) 513–524. doi:10.1016/J.EXPTHERMFLUSCI.2006.06.001.
URL https://www.sciencedirect.com/science/article/pii/S0894177706000884
[24] M. Vanierschot, Fluid mechanics and control of annular jets with and without swirl, Ph.D. thesis, KU Leuven (2007).
URL https://lirias.kuleuven.be/retrieve/67461
[25] M. Vanierschot, E. Van Den Bulck, Influence of the nozzle geometry on the hysteresis of annular swirling jets, Combustion Science and Technology 179 (8) (2007b) 1451–1466. doi:10.1080/00102200601147856.
URL http://www.tandfonline.com/doi/abs/10.1080/00102200601147856
[26] N. K. Singh, K. Ramamurthi, Formation of Coanda jet from sharp-edged swirl nozzle with base plate, Experimental Thermal and Fluid Science 33 (4) (2009) 675–682. doi:10.1016/J.EXPTHERMFLUSCI.2009.01.008.
URL https://www.sciencedirect.com/science/article/pii/S0894177709000120
[27] A. Valera-Medina, H. Baej, Hydrodynamics During the Transient Evolution of Open Jet Flows from/to Wall Attached Jets, Flow, Turbulence and Combustion 97 (3) (2016) 743–760. doi:10.1007/s10494-016-9718-5.
URL http://link.springer.com/10.1007/s10494-016-9718-5
[28] N. Syred, M. Abdulsada, A. Griffiths, T. O'Doherty, P. Bowen, The effect of hydrogen containing fuel blends upon flashback in swirl burners, Applied Energy 89 (1) (2012) 106–110. doi:10.1016/J.APENERGY.2011.01.057.
URL https://www.sciencedirect.com/science/article/pii/S0306261911000754
[29] M. Vanierschot, K. Van Dyck, P. Sas, E. Van den Bulck, Symmetry breaking and vortex precession in low-swirling annular jets, Phys Fluids 26 (2014) 105110.
[30] F. Moisey, pivmat (2017).
URL http://www.fast.u-psud.fr/pivmat/
[31] M. Sieber, C. O. Paschereit, K. Oberleithner, Spectral proper orthogonal decomposition, Journal of Fluid Mechanics 792 (2016) 798–828.
[32] M. Vanierschot, G. Ogus, Experimental investigation of the precessing vortex core in annular swirling jet flows in the transitional regime, Experimental Thermal and Fluid Science 106 (2019) 148–158.
[33] M. Vanierschot, E. Van den Bulck, Numerical study of hysteresis in annular swirling jets with a stepped-conical nozzle, International Journal for Numerical Methods in Fluids 54 (3) (2007c) 313–324. doi:10.1002/fld.1400.
URL http://doi.wiley.com/10.1002/fld.1400
[34] S. Abdurakipov, L. Chikishev, PIV study of vortex breakdown in low- and high-swirl flames in a model combustor, in: 10th International Symposium on Particle Image Velocimetry, 2013.
URL https://repository.tudelft.nl/islandora/object/uuid%3A2d79314c-bbde-402f-b760-06d80f60eda3
[35] M. Li, Y. Tong, J. Klingmann, M. Thern, Experimental Study of Hydrogen Addition Effects on a Swirl-Stabilized Methane-Air Flame, Energies 10 (11) (2017) 1769. doi:10.3390/en10111769.
URL http://www.mdpi.com/1996-1073/10/11/1769